Insights into the real part of natural sea spray aerosol refractive index in the Pacific Ocean

Chengyi Fan[1], Bishuo He[1], Shuqi Guo[1], Jie Qiu[1], Chunsheng Zhao[1]

[1]Department of Atmospheric and Oceanic Sciences, School of Physics, Peking University, Beijing 100871, China

Correspondence to: Chunsheng Zhao (zcs@pku.edu.cn)

Abstract. Sea spray aerosols (SSA) play a pivotal role in influencing radiative effects over oceanic regions, making it essential to accurately quantify their optical properties, particularly the real part of the refractive index (RRI) under varying relative humidity (RH) conditions. This study employs an aerosol optical tweezers (AOT) system coupled with Mie scattering theory to precisely measure the RRI of sea spray aerosols at 650 nm across a range of RH levels. First, standard ammonium sulfate particles were used to validate the AOT measurements against thermodynamic models and previously established parameterizations, confirming the reliability of the optical tweezers' measurements. Measurements of SSA from offshore and open-sea samples show consistent RRI values, independent of seawater salinity, with artificial sea salt particles effectively representing the optical properties of real SSA at RH > 70%. A least-squares linear regression scheme linking RRI and RH was developed, allowing for accurate RRI estimation under varying RH conditions. Additionally, our scheme's intercept at RH = 0 potentially represents the molten-state RRI for sea spray aerosols, validated against standard particles. Results highlight that traditional volume-weighted mixing rules underestimate RRI and aerosol optical depth (AOD), thus reinforcing the need for direct measurement-based parameterizations. This study underscores the importance of accurately representing sea spray aerosols' radiative properties in climate models. We suggest incorporating the proposed linear regression scheme into aerosol and radiative transfer models to improve model accuracy and enhance the understanding of the effects of sea spray aerosols on radiative processes.

1 Introduction

The real part of the refractive index (RRI, n) is a fundamental optical parameter that governs aerosol particles' interaction with light, such as light scattering coefficients, single scattering albedo, and backscatter fraction (Wang and Rood, 2008). It plays a pivotal role in atmospheric models and remote sensing applications, where accurate RRI values are needed to assess aerosol impacts on climate (Kahn et al., 2010; Myhre et al., 2013; Zhao et al., 2017). Despite its importance, the refractive index of aerosols remains inadequately constrained, especially under conditions of elevated relative humidity (RH), creating significant uncertainties in understanding how aerosols affect radiative forcing (Wang and Rood, 2008; Zarzana et al., 2014; Zhao et al., 2019).

Sea spray aerosols (SSA), formed when strong winds break ocean surface waves and entrain air into seawater, stand out due to their significant global contribution to light scattering (Richter and Veron, 2016). Globally, the annual flux of SSA is estimated between 1 and 3×10^{16} g, making it one of the most significant primary aerosol sources (O'Dowd and de Leeuw, 2007; Ault et al., 2013; Quinn et al., 2017). SSA, which consists primarily of sea salt, organic material, and seawater, plays a crucial role in the Earth's radiation budget. These particles directly scatter solar radiation at the top of the atmosphere (TOA), with global average scattering radiation ranging from -0.08 to -6 W/m^2. The large uncertainties in this range arise from variability in sea salt load and the limited availability of optical property data for SSA, such as the RRI (Haywood et al., 1999; de Leeuw et al., 2011; Aldhaif et al., 2018). In addition, due to their hygroscopicity, SSA can act as cloud condensation nuclei or ice nuclei, indirectly affecting cloud formation and radiative forcing (de Leeuw et al., 2011; Quinn et al., 2017). Despite the critical role of SSA in climate processes, uncertainties in the optical properties of these particles, particularly RRI, remain a significant challenge. Perturbations of just 0.05 in n can result in approximately 10% changes in aerosol optical depth (AOD), emphasizing the need for accurate SSA refractive index data (Aldhaif et al., 2018).

However, current measurement techniques, such as thin disk bulk measurement and electrodynamic balance suspension, suffer from limitations including poor representation of natural SSA and assumptions about particle density, which can introduce substantial errors (Volz, 1972; Tang et al., 1997). Moreover, model calculations typically estimate the refractive index of SSA using the RRI of pure sea salt and apply volume-weighted mixing rules based on known component properties (Shettle and Fenn, 1979; Wang et al., 2019). While computationally efficient, this approach risks large inherent errors due to its divergence from physical reality. Therefore, direct measurements of the RRI of real SSA under varied atmospheric conditions are essential to reduce these uncertainties and improve climate model accuracy.

In addition to the methodological challenges, SSA's chemical composition significantly affects its refractive index (Tang et al., 1997; Ming and Russell, 2001). While sea salt constitutes the majority of SSA, organic compounds are also present, especially in submicron particles (O'Dowd et al., 2004; Gantt and Meskhidze, 2013). These components' concentrations and relative proportions vary across oceanic regions and change seasonally (O'Dowd et al., 2004; Rhein et al., 2013). Furthermore, due to the inherent similarity between the composition of SSA and the seawater from which it is derived, SSA from offshore and open-sea areas may display distinct properties (Lewis and Schwartz, 2004; Keene et al., 2007). It is also critical to evaluate whether artificial sea salt particles, commonly used in laboratory settings, can accurately represent natural SSA. These uncertainties contribute to the difficulty of estimating SSA's true radiative effects (Gantt and Meskhidze, 2013).

To address these gaps, we developed an aerosol optical tweezers (AOT) system to directly measure the RRI of SSA particles under controlled RH in real time. This system overcomes the limitations of bulk measurement methods by allowing us to isolate individual SSA particles produced by an ultrasonic nebulizer through the pattern of jet drops (Richter and Veron, 2016). It provides accurate, in situ measurements without the need for density assumptions and the particles generated in this manner are micron-sized, exhibiting a similar size and composition to supermicron SSA. In

contrast to another well-established nephelometer method for measuring aerosol scattering coefficients, optical tweezers, circumvent the potential inconsistencies arising from ensemble averaging and multi-particle interactions by capturing and measuring individual particles. This ensures that each measurement reflects the intrinsic optical properties of individual particles and reveals the physicochemical characteristics of particles from a distinct perspective, particularly the influence of humidity on the refractive index.

In this study, we conducted experiments using both artificial sea salt and natural SSA particles in the coarse mode, which contribute significantly to the total SSA mass and radiative forcing (Kleefeld et al., 2002). Our primary objective was to investigate potential differences in the refractive index of SSA generated from offshore and open-sea regions in the Pacific Ocean, though in a narrow range at 650 nm. Additionally, we aimed to assess the suitability of artificial sea salt particles as proxies for natural SSA. This research represents the first use of the AOT system to directly measure the RRI of natural SSA and sea salt particles. Furthermore, it is the first study to compare the optical properties of SSA from offshore and open-sea regions within the Pacific, providing valuable insights into the potential optical differences and their implications for the Earth's radiative balance. We also provide direct measurements of the RRI of actual SSA at different RHs, along with parameterization schemes. Compared to the traditional volume-weighted mixing rule, this approach can offer better constraints on the radiative uncertainties of SSA in climate models.

This article is structured as follows. In Section 2, we describe the materials and methods, including details of the seawater sampling, aerosol generation, and the AOT system used for measuring the RRI of sea spray aerosols at varying relative humidity levels. Section 3 presents the results and discussion, where we validate the accuracy of the AOT measurements, compare observed RRI data for offshore and open-sea SSA, and develop a parameterization scheme linking RRI to relative humidity. We also evaluate the limitations of traditional volume-weighted mixing rules by comparing them with our measured data. In Section 4, we provide conclusions, highlighting the significance of these findings for climate models and radiative transfer processes, and suggest potential directions for future research to further enhance our understanding of SSA's radiative effects.

2 Methodology

2.1 Samples and chemicals

The seawater samples used in this experiment are identical to those used in previous research and are briefly summarized here (Qiu et al., 2024). Samples were collected from surface waters (<5 m depth) at various locations along the research vessel "*TAN* KAH *KEE*" cruise track (Fig. 1). The South China Sea sample was obtained during the KK1702 expedition in September 2017, while the remaining six samples were collected during the NORC2022-306 expedition between June and July 2022. The South China Sea and Kuroshio samples are categorized as offshore waters, while the other five stations are considered open-sea regions. The primary difference between the offshore and open-sea samples is salinity, with offshore regions closer to land

exhibiting lower salinity due to freshwater dilution. The salinity of the seawater samples, which ranged from 34‰ to 35‰, was automatically measured onboard during sampling and is depicted in Table S1. The seawater samples were collected in 125 mL high-density polyethylene (HDPE) bottles and frozen immediately at -20°C, effectively preserving the integrity of the samples until analysis and ensuring reliable and accurate results for our research. It should be noted that salt exclusion may occur during freezing, concentrating dissolved salts in the remaining liquid as the ice forms. To minimize this effect, we allowed the samples in sealed bottles to thaw completely at room temperature and mixed the samples thoroughly before measurement. We believe this slow thawing process ensures minimal impact on sample composition and subsequent results.

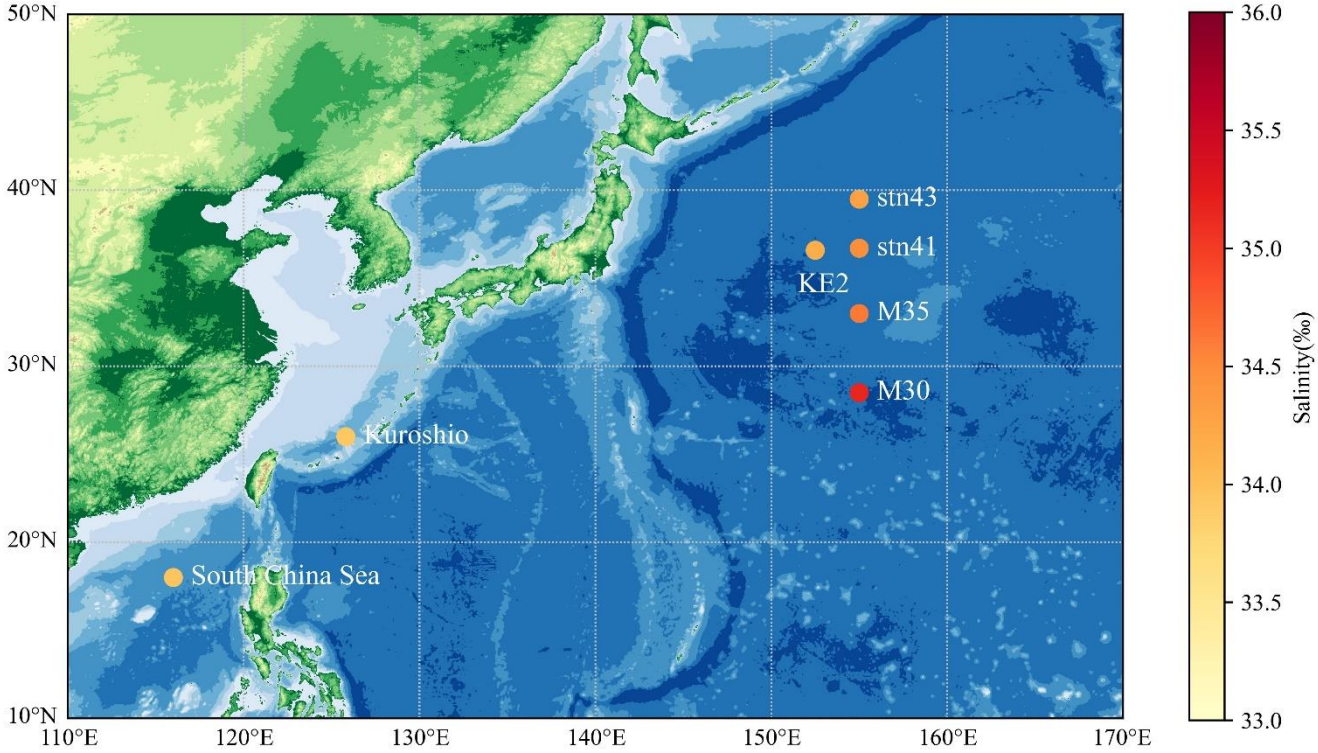

Figure 1. Map showing specific stations where surface seawater was sampled, with color representing its salinity. Symbols plotted on the map represent the sampling locations.

Besides the natural seawater samples, inorganic reference solutions were prepared using artificial sea salt (ASTM D 1141-98; Lake Products Company LLC), high-purity ammonium sulfate ($(NH_4)_2SO_4$, 99.0% AR; Sinopharm Chemical Reagent Co., Ltd.) and sodium chloride (NaCl, 99.5% AR; Shanghai Titan Scientific Co., Ltd.). The artificial sea salt contains 58.490% mass of sodium chloride (refractive index, RI = 1.544) along with other salts such as magnesium chloride, sodium sulfate, and calcium chloride, each contributing different refractive indices. Ultrapure water (18 MΩ·cm; SIMGEN; Hangzhou SIMGEN Biotechnology Co., Ltd.) was utilized to prepare nebulization solutions.

2.2 Aerosol optical tweezer system

The AOT system used in this study has been described in previous literature (Cai et al., 2018; Qiu et al., 2024; Preston and Reid, 2013) and is briefly summarized here. As shown in Fig. 2, the system employs a semiconductor laser (Laser Quantum, Opus-6000, 532 nm) that produces a Gaussian beam with an initial power output of approximately 200 mW. This beam is collimated, expanded, and focused using convex lenses before being directed through an oil immersion objective lens (Olympus UIS2 PlanCN, 100×, 1.25 N.A.). A custom-built sample chamber is utilized to confine aerosol droplets generated by a medical ultrasonic nebulizer (Yuyue 402AI model), which can simulate the formation of SSA using small amounts of seawater. The chamber's bottom aperture allows the laser to pass through, applying a gradient force that stabilizes the droplet within the trap and induces its Raman signal. The scattered Raman signal from the droplet is collected by a spectrograph (Zolix Omni λ-300i, 1200 grooves mm−1 grating) and a CCD camera (Andor Solis 256, pixel array 1024 × 256) at a recording rate of 1 frame per second, enabling precise measurements of the particle's refractive index subsequently.

It is important to note that the nebulizer generates fine bubbles in the seawater solution through ultrasonic vibration. When these bubbles grow and burst, the resulting surface cavities induce surrounding liquid flow and splashing, creating jet drops. This process simulates the jet drop mechanism in forming real sea spray aerosols, producing micron-sized particles. In our experiments and subsequent fitting calculation, the AOT system usually stabilized particles within the size range of 3-7 microns, aligning with the expected particle size generated by the nebulizer. Real sea salt aerosols are typically categorized into small, medium, and large SSA, with the medium SSA size range being 1-25 microns (Lewis and Schwartz, 2004). These particles, mainly produced through the jet drop mechanism, contribute significantly to sea salt aerosol mass and optical scattering. Therefore, using the particles generated by the nebulizer as surrogates for real SSA to study radiative properties is a reasonable approach. Regarding chemical composition, while organic components can make up over 50% of the dry mass of submicron SSA, they account for less than 5% of supermicron SSA particles (de Leeuw et al., 2011). In our study, reducing the environmental relative humidity (RH) to 70% still showed no detectable C-H peaks (around 2800-3100 cm^{-1}) in the Raman spectra (Fig. S1), indicating that the organic content in the micron-sized particles is minimal, similar to that of real supermicron SSA. Given that the solution used for aerosol generation was real seawater and the organic content is negligible, the chemical

composition of the particles generated by the nebulizer is also unlikely to differ significantly from real supermicron SSA.

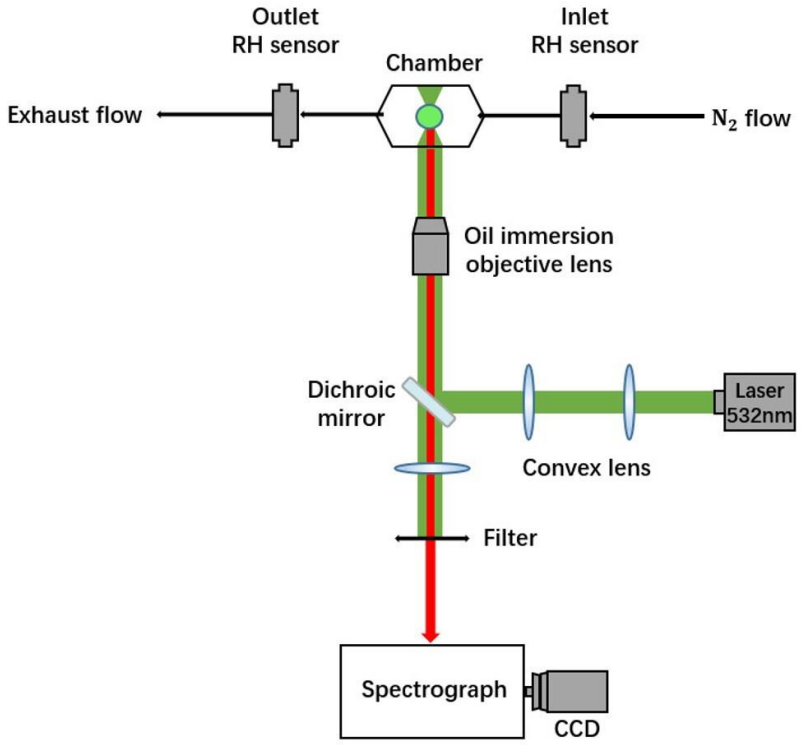

Figure 2. Schematic of the optical layout for aerosol optical tweezer.

The relative humidity inside the sample chamber is controlled by manipulating the ratio of dry and water-saturated nitrogen gas flows, which are thoroughly blended before being introduced into the chamber. The gas flow rates are regulated in real time using mass flow controllers (Dmass, DFC10-1/4-N2-3000SCCM-B01). Two humidity-temperature probes (ROTRONIC, HC2A-S) are positioned at the inlet and outlet of the chamber to monitor RH and temperature continuously throughout the experiments. All measurements are carried out at room temperature (20 °C) and under ambient pressure conditions. The uncertainty in RH data, attributed to temperature fluctuations, is estimated to be ±0.16% during the experiment.

2.3 Characterization of the real part of the refractive index

Once the SSA particles are stably trapped by the optical tweezers, their radius and refractive index are determined simultaneously by analyzing the Raman spectra collected by the spectrometer. The method is based on the principle that when the wavelength of light is comparable to the particle size, the micron-sized spherical droplets trapped by the optical tweezers

function as high-quality optical microcavities (Preston and Reid, 2013). At specific wavelengths, the Raman scattered light undergoes multiple total internal reflections within the spherical particle, forming standing waves with optical paths equal to integer multiples of the wavelength. These sharp, narrow spontaneous Raman scattering peaks enhanced by the cavity resonances and superimposed on the broad spontaneous Raman scattering background, as shown in Fig. 3, are known as Whispering Gallery Modes (WGMs) (Benner et al., 1980). The wavelengths of these WGMs are dependent on the particle's size, morphology, and refractive index.

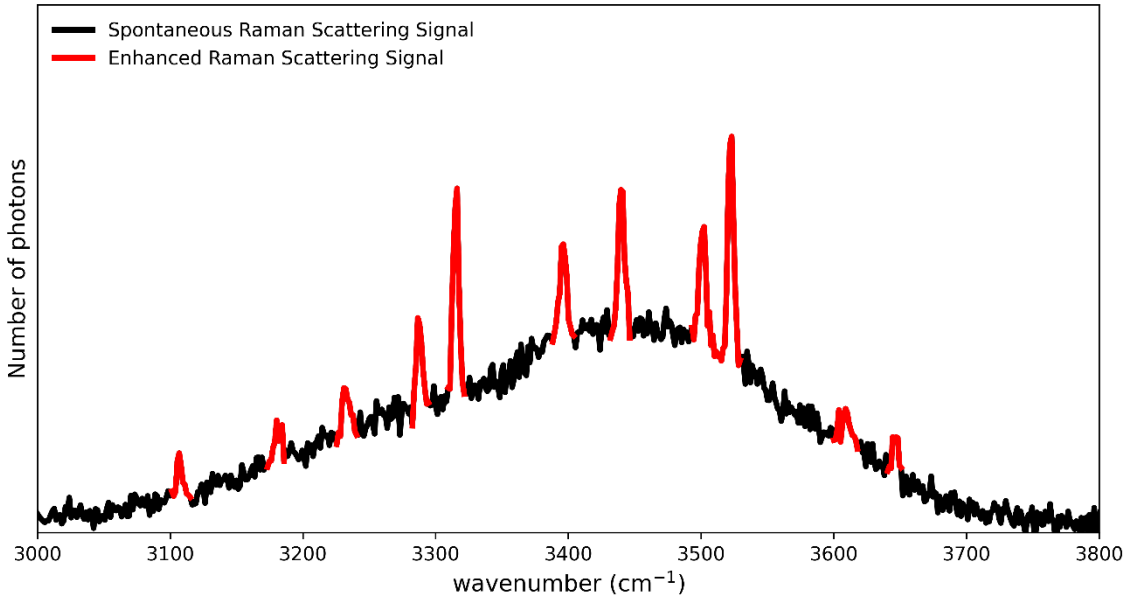

Figure 3. Example of enhanced Raman scattering signal on the broad spontaneous Raman scattering background.

Each WGM is characterized by three parameters for spherically symmetric particles: mode number, mode order, and polarization state (either Transverse Electric (TE) or Transverse Magnetic (TM) mode), which corresponds to Mie scattering theory. In this study, all measured refractive indices are at the wavelength of 650 nm using the fitting method of Preston and Reid (2013). Briefly, a table of resonance size parameters is constructed for different refractive indices and WGMs. Experimental spectral peak values are then converted into size parameters for the given radius. Next, a parameter space of radius and refractive index is explored to minimize the total error between the calculated and observed peak positions under dispersion-free conditions. Following this, a narrow range of dispersion is considered, and a new table is generated for a smaller parameter space, with fitting performed to minimize the overall error and obtain the best parameters. By selecting appropriate parameter boundaries and intervals, the Mie scattering series can be optimized using a recursive approach, enabling the calculation of particle size and the RRI. Given that the imaginary part of SSA's refractive index is negligible, the typical

precision of the fitted particle size and RRI derived from this method can reach ±20 nm and ±0.005, respectively and an example of fitting is shown in Fig. S2.

3 Results and discussion

3.1 Validation of the method for measuring the real part of the refractive index using aerosol optical tweezers

To validate the accuracy of the RRI obtained using the AOT system combined with Mie theory fitting, this study first measured the RRI of ammonium sulfate particles under different RH conditions. These results were then compared with previously reported data and the E-AIM IV (Extended Aerosol Inorganics Model, version IV) thermodynamic model, as shown in Fig. 4 (Wexler and Clegg, 2002; Cotterell et al., 2017). The E-AIM IV model provides solute concentration and water content in particles at specified RH, which, combined with the molar refraction approach, enables the calculation of the corresponding RRI as Figure S3. and Table S2. shown (Moise et al., 2015; Cai et al., 2016). Compared to volume-weighted and mass-weighted mixing rules, the molar refraction approach has the advantage of theoretical support in physical chemistry, specifically through the additive property of molar refraction as a molar quantity. The average error for the molar refraction method is within 0.75% and is adopted as uncertainty here (Wang and Rood, 2008). Figure 4 demonstrates that the RRIs obtained by the AOT and the E-AIM IV model are consistent within this uncertainty range. Although the E-AIM IV model underestimates the RRI to some extent at RH below 75%, this may be because the data of the E-AIM IV model are extrapolated from unsaturated solutions, which can introduce a certain bias when predicting the composition of supersaturated particles. This, in turn, leads to discrepancies between the calculated and measured RRI values.

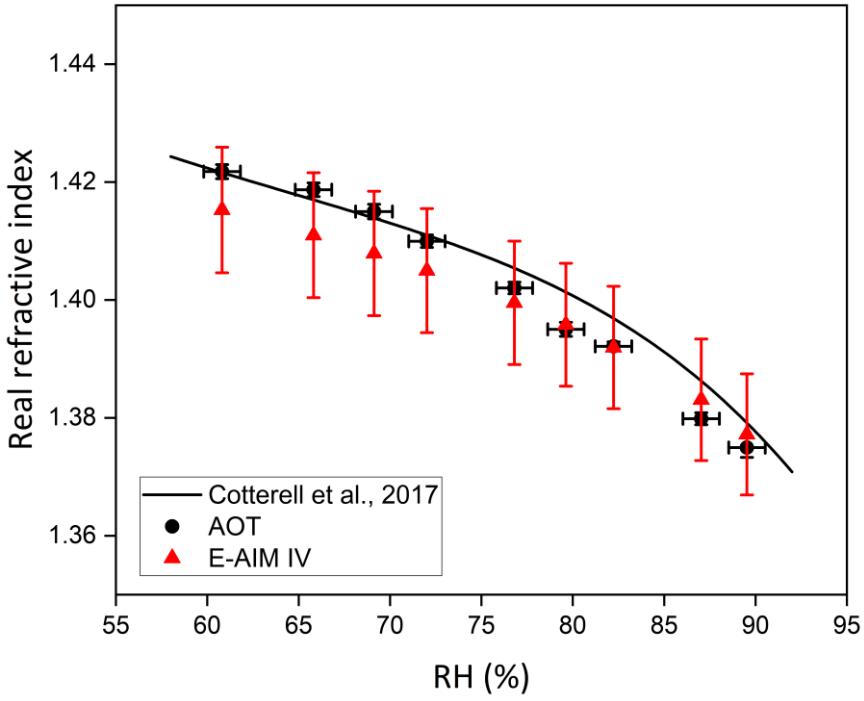

Figure 4. Variation of the real part of the refractive index of ammonium sulfate particles with RH. Data from the E-AIM IV model at 293.15 K and the previous parameterization scheme by Cotterell et al. (2017) are shown for comparison.

Cotterell et al. (2017) provided a parameterization of ammonium sulfate RRI under different RH and wavelength conditions, showing excellent agreement with the AOT within the 60-75% RH range. At RH above 75%, the values provided by the parameterization are slightly higher than those measured by the AOT (about 0.5%). This discrepancy was also observed by Cotterell et al. (2017) and attributed to the lack of measurement data at wavelengths longer than 600 nm, which leads to inherent overestimations in the parameterization at these wavelengths. Additionally, errors in the humidity-temperature probes and inconsistencies in environmental conditions may also contribute to this deviation. Therefore, by comparing the RRI of ammonium sulfate particles measured by the AOT, calculated using the E-AIM IV model, and parameterized by Cotterell et al. (2017), we confirmed the reliability of RRI measurements obtained from the AOT system.

3.2 Results of the real part of the refractive index

A series of experiments were conducted on seawater samples from seven sampling stations to obtain the Raman spectra of SSA particles. Using Mie fitting, the diameter and RRI of the particles were determined. At the end of each experiment, the used seawater was discarded, and all instruments were thoroughly cleaned before generating new particles with fresh seawater.

Each RRI result was derived from Raman spectra collected over at least 3 h (18,000 frames) of equilibrium state, and the average RRI was calculated along with 1 standard deviation.

The RRI results for SSA particles from the seven stations, along with the corresponding salinity data of their bulk seawater samples, are summarized in Fig. 5. At RH = 90%, the mean RRI for offshore SSA is 1.366, while for open-sea SSA is 1.367, with a standard deviation of 0.0012. At RH = 80%, the mean RRI for offshore SSA is 1.380 and 1.381 for open-sea SSA, with a standard deviation of 0.0008. At RH = 75%, the mean RRI for offshore SSA is 1.385, while for open-sea SSA is 1.386, with a standard deviation of 0.0018. Data at lower RH were not directly measured because SSA particles shrink as they lose water, eventually becoming too small to be stably captured by the AOT system. Additionally, WGMs indicating a uniform spherical particle shape remained present throughout the capture of SSA particles as shown in Fig S1.

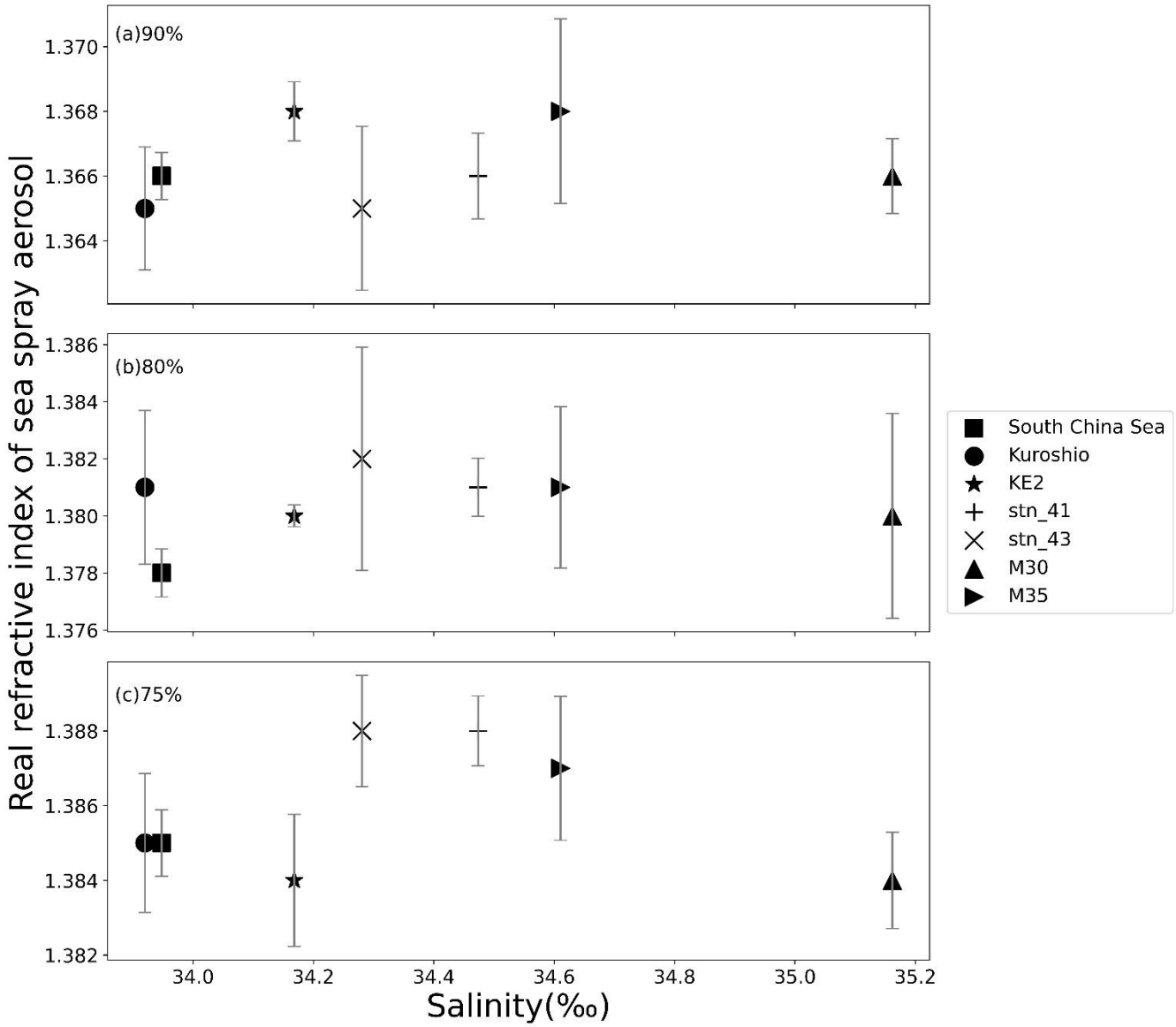

Figure 5. RRI values of sea spray aerosols generated from seawater samples of seven stations at different RH levels: 90% **(a)**, 80% **(b)**, 75% **(c)**. The x-axis represents the salinity of the bulk seawater samples.

215

Across the three RH conditions, the SSA particles exhibit a dependence on ambient RH. A clear trend is observed where a decrease in RH corresponds to an increase in the RRI, consistent with previous findings (Tang and Munkelwitz, 1994; Cotterell et al., 2017). This trend arises from the particles' hygroscopic nature: as RH decreases, water, which has an RRI of 1.333, is lost, leading to an increased overall RRI, as the refractive indices of dissolved salts are generally higher.

Comparing the RRI data for offshore and open-sea SSA in this study, it is found that within the margin of error, the RRI values for offshore and open-sea SSA are consistent, showing no significant dependency on the salinity of the source seawater. This finding aligns with previous research showing that the hygroscopic properties of offshore and open-sea SSA are nearly identical (Qiu et al., 2024). Reich et al. (2023) reached a similar conclusion, noting that variations in seawater salinity do not affect droplets' hygroscopic properties when ion relative abundances are the same and small changes in the relative abundance of ions in seawater have no significant effect on the hygroscopicity of the particles. This may be similar to the RRI, given the nearly identical hygroscopic growth factors and solute refractive indices for both types of SSA.

3.3 Parameterization of the real part of the refractive index and relative humidity

In this study, we also measured the RRI of artificial sea salt particles at RH levels of 75-90%, comparing these values to those of real SSA measured from samples at the seven stations (Fig. 6). Results show that within this RH range, the RRI values of real SSA are highly consistent with those of artificial sea salt particles. At RH > 60%, both real SSA and artificial sea salt particles display a well-defined linear relationship between RRI and ambient RH.

Given the identical RRI values of offshore and open-sea SSA, a combined least-squares linear regression scheme of the RRI for real SSA as a function of RH is developed:

$$n = -1.298e^{-3} \times RH + 1.484 \quad (1)$$

The coefficient of determination, R^2, for this scheme, is 0.974, and the p-value for slope and intercept is $3.59e^{-26}$ and $1.19e^{-61}$ respectively, indicating a statistically significant relationship. This regression scheme provides an accurate estimation of n across various RH levels, particularly at the typical marine relative humidity where SSA exists. The 95% confidence interval for the slope and intercept ranges from $-1.375e^{-3}$ to $-1.220e^{-3}$ and 1.478 to 1.490, respectively. The slope reflects the hygroscopic growth ability of particles to some extent. A stronger hygroscopic ability of the components leads to greater water uptake with increasing RH, resulting in a more pronounced decrease in refractive index, and consequently, a larger absolute value of the slope. The intercept, corresponding to RH = 0, is interpreted as potential RRI of molten SSA particles at 20 °C if we assume that the sea salt particles do not undergo efflorescence and remain in a dissolved molten state. Although the assumed molten state may not occur in the real atmosphere, the extrapolated values still provide a basis for further analysis. Furthermore, the linear relationship and parameterization scheme, which can be incorporated into climate models, are valid and align well with measurements in marine environments with RH > 60%. On the other hand, while structural changes may occur, the RRI of molten sea salt appears to closely match the dry sea salt refractive index of 1.49 reported in previous studies (Shettle and Fenn, 1979).

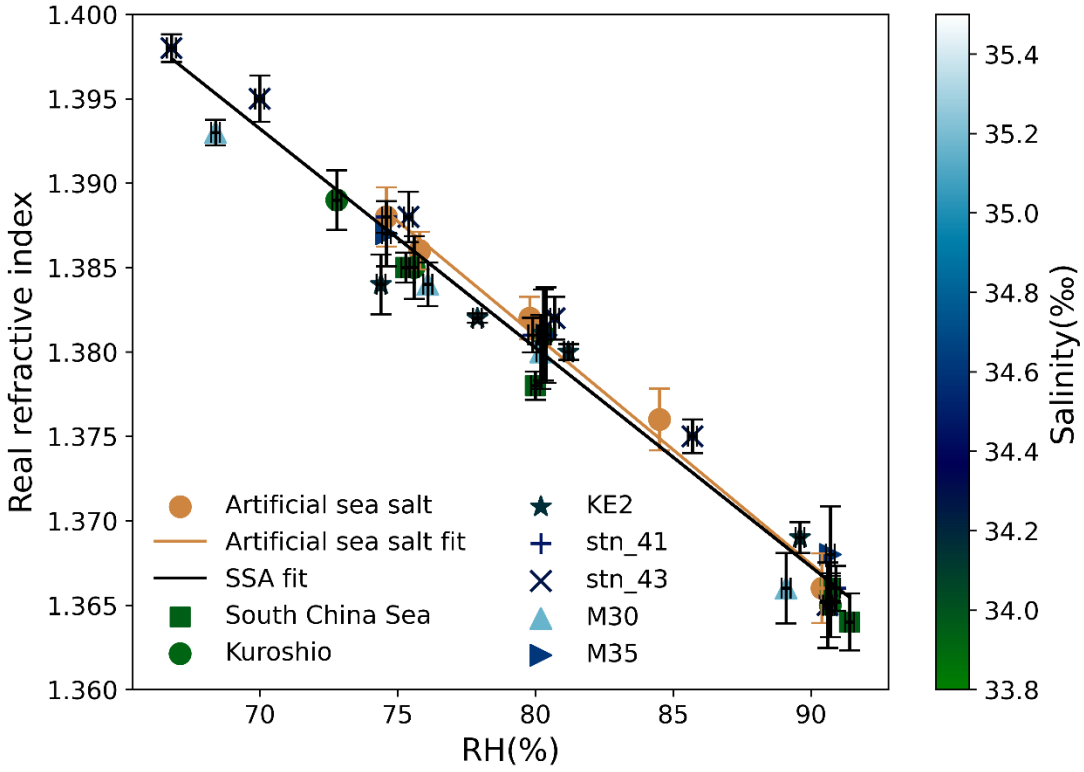

Figure 6. The relationship between n and RH for real SSA and artificial sea salt particles. The color of the real SSA data points indicates the salinity of the bulk seawater sample at each station. Lines are the linear regression of sea salt and sea spray aerosol data.

The least-squares linear regression scheme for the RRI of artificial sea salt particles with RH is:

$$n = -1.355e^{-3} \times RH + 1.489 \quad (2)$$

With an R^2 of 0.990 and the p-value of 4.22e^{-4} and 1.72e^{-7} for slope and intercept respectively, the scheme shows a strong fit. The 95% confidence interval for the slope ranges from -1.604e^{-3} to -1.105e^{-3}. According to the method proposed in this study, the RRI for molten artificial sea salt particles is estimated to be 1.489 (1.469-1.509), differing by only 0.4% from the RRI of real SSA. Given the close match between their RRI values across various RH conditions, we conclude that artificial sea salt particles are a suitable proxy for representing the radiative properties of real SSA. However, the RRI of molten sodium chloride, extrapolated from high-temperature data to 20 °C, is 1.513 (Janz, 1967), and is 1.42% higher than that of SSA. This is likely due to the presence of lower refractive index compounds like sodium sulfate in natural sea salt and indicates that sodium chloride is not a perfect substitute for SSA in studies of radiative properties when greater accuracy is required. Therefore, we recommend using artificial sea salt instead individual sodium chloride particles as a substitute for real SSA in the laboratory or radiative transfer model.

3.4 Comparison of measured RRI data with the volume-weighted mixing rule

In the Community Earth System Model (CESM), Ghan and Zaveri (2007) implemented a volume-weighted approach to calculate the RRI of SSA at various RH levels:

$$n_e = \frac{\sum V_i n_i}{\sum V_i} = n_w + (n_0 - n_w)\frac{r_d^3}{r_w^3} \quad (3)$$

where n_e represents the effective RRI, n_0 is the RRI of sea salt, n_w is the RRI of water, r_d refers to the dry particle radius of the particle, r_w refers to the equilibrated particle radius at given RH, and V_i refers to the volume of the ith component. This volume-weighted approach is convenient as it does not require density or mass data for the particles, making it widely used in various models. However, given that this method lacks a physical basis as an empirical formula, it is necessary to validate the accuracy of the volume-weighted approach using the AOT-measured data.

For sea spray aerosols, the particle radius at RH = 80% is approximately twice the dry radius, compensating for the AOT system's inability to measure dry particle size (Lewis and Schwartz, 2004; Qiu et al., 2024). Additionally, assuming that SSA components can be represented by artificial sea salt due to the similar RRI across various RH, we considered the main components, sodium chloride, magnesium chloride, and sodium sulfate only, with original mass fractions of 58.49%, 26.46%, and 9.75%, respectively. Using the fitting relationship for density based on solute mass fraction, the densities of these components in the molten state at room temperature are determined as 2.088, 2.492, and 2.540 g/cm³, respectively (Tang et al., 1997; Clegg and Wexler, 2011). Applying the ideal density mixing rule, the density of molten sea salt is then calculated to be 2.236 g/cm³. Similarly, the density of dry sea salt is calculated as 2.297 g/cm³, which is used to convert the volume between dry and molten sea salt. The RRI and particle size data for offshore, open-sea SSA, and artificial sea salt particles from our AOT measurements are then input into volume-weighted calculation, discrepancies arise as shown in Table 1, where r_m refers to the molten particle radius of the particle. Specifically, n_e from the volume-weighted approach underestimates n values by up to 0.032, approximately 2.32%. Previous studies incorporating field observations and models have shown that as n of SSA varies from 1.42 to 1.60, it can introduce a 41.9% error in aerosol optical depth (AOD) (Aldhaif et al., 2018). Therefore, at RH = 75%, our results indicate that using the volume-weighted approach may lead to an AOD underestimation of up to 7.4% as a simple estimate, significantly impacting estimates of SSA radiative forcing.

Table 1. Summary of RRI Calculation Results.

Sample	Offshore (South China Sea)	Open sea (M35)	Artificial Sea Salt
r_d(nm)	2118	2132	2335
r_m(nm)	2137	2151	2356
n_0	1.484	1.484	1.489

r_w_90%(nm)	4813	4794	5336
n_e_90%	1.346	1.347	1.346
n_{AOT}_90%	1.366	1.368	1.365
Absolute Diff. 90%	0.020	0.021	0.019
Relative Diff. 90%	1.45%	1.56%	1.36%
r_w_75%(nm)	4056	4054	4474
n_e_75%	1.355	1.356	1.356
n_{AOT}_75%	1.385	1.387	1.388
Absolute Diff. 75%	0.030	0.031	0.032
Relative Diff. 75%	2.16%	2.27%	2.32%

As Table 1 shows, the RRI values derived from the volume-weighted mixing rule are not accurate across varying RH levels for SSA. To reduce uncertainties in the radiative contributions of SSA and other aerosols, it is critical to incorporate experimentally measured RRI data into climate models rather than relying solely on volume-weighted estimates. We recommend embedding our least-squares linear regression scheme of n as a function of RH from the AOT measurements directly into aerosol models or remote sensing algorithms. This approach could significantly enhance our understanding of SSA's impact on surface radiative processes.

4 Summary and Conclusions

Sea spray aerosols are major contributors to radiative effects over oceanic regions (Murphy et al., 1998; Haywood et al., 1999), making it essential to consider their impacts on radiative transfer in aerosol remote sensing and ocean color atmospheric correction algorithms (He et al., 2012; Sayer et al., 2012). However, accurately quantifying SSA's optical properties, particularly the real part of the refractive index, under varying ambient RH conditions remains a significant challenge. This lack of precise RRI data for SSA under diverse RH conditions limits our ability to accurately represent their radiative impacts in climate models.

Using the aerosol optical tweezers system combined with Mie scattering theory, we accurately measured the size and RRI of trapped particles. In this study, we first validated RRI measurements of ammonium sulfate particles using the E-AIM IV thermodynamic model, molar refractivity, and previously published parameterizations based on measured data, ensuring the reliability of the optical tweezer-derived RRI values. Subsequently, we measured n values of SSA at various RH levels at two

offshore sites in the South China Sea and Kuroshio Current and five open-sea sites in the western Pacific. Results indicate that n values for offshore and open-sea SSA are consistent within the error range. Moreover, under RH > 70% experimental conditions, artificial sea salt particles effectively represent n values of real SSA, suggesting their suitability in radiative transfer models as a proxy for real SSA rather than pure NaCl particles.

By analyzing the relationship between the real part of the refractive index of SSA and RH, we established a least-squares linear regression scheme linking these variables. This parameterization allows future researchers to estimate the RRI of sea spray aerosols directly based on ambient RH. Additionally, our study proposes that the intercept value of this scheme, corresponding to RH = 0, can potentially represent the RRI of particles in the molten state. Optical tweezer measurements yield a n value of 1.484 for real SSA in the supermicron range, which also appears to closely match prior field observations of the RRI of accumulation-mode SSA (Shettle and Fenn, 1979; Shepherd et al., 2018), demonstrating the potentially wide applicability of our results.

Combining optical tweezers data with the volume-weighted mixing rule for calculating RRI shows that traditional volume-weighted methods may underestimate n value by up to 2.32% compared to our results, potentially leading to a 7.4% underestimation of SSA aerosol optical depth. This suggests that the volume mixing rule cannot accurately represent SSA radiative properties, and actual measured values should be used instead. Our least-squares linear regression scheme enhances the accuracy of the RRI of SSA under different RH conditions, especially at the typical marine RH, making it suitable for calculating the RRI of SSA in the ambient atmosphere and recommending its application in radiative transfer models.

Given the increasing relevance of climate change, this study highlights the importance of accurately representing SSA radiative properties in global climate models. This insight can reduce uncertainties in aerosol radiative forcing, aiding in climate prediction. While our research advances the understanding of the scattering characteristics of offshore and open-sea SSA in the supermicron range, it is important to note that our measurements cover RRI at a single wavelength only. To further quantify the radiative contributions of SSA and other aerosols, measurement methods across the entire solar spectrum should be urgently developed. Additionally, to fully reveal the complexity of scattering by natural sea spray aerosols with significant organic content, further research is required on submicron natural sea spray aerosols.

Code availability

Codes used in this study are available on request from the corresponding author (email: zcs@pku.edu.cn).

Data availability

The data presented in the study can be found at https://pan.baidu.com/s/1kfOTDO5EDY29baoBuIwc_g?pwd=4akw

Author contribution

CF and JQ put forward the idea. CF performed the experiments with the help of SG. CF analyzed the data with the technical support of BH. CF wrote the manuscript. C.Z. reviewed and revised the manuscript.

Competing interests

The authors declare that they have no conflict of interest.

Acknowledgements

We gratefully acknowledge the financial support of the National Natural Science Foundation of China (42275070) and the technical support of Chen Cai. During the preparation of this work, the authors used ChatGPT to polish the paper. After using this tool, the authors reviewed and edited the content as needed and took full responsibility for the publication's content.

References

Aldhaif, A. M., Stahl, C., Braun, R. A., Moghaddam, M. A., Shingler, T., Crosbie, E., Sawamura, P., Dadashazar, H., Ziemba, L., Jimenez, J. L., Campuzano-Jost, P., and Sorooshian, A.: Characterization of the Real Part of Dry Aerosol Refractive Index Over North America From the Surface to 12 km, J. Geophys. Res.-Atmos., 123, 8283–8300, https://doi.org/10.1029/2018JD028504, 2018.

Ault, A. P., Moffet, R. C., Baltrusaitis, J., Collins, D. B., Ruppel, M. J., Cuadra-Rodriguez, L. A., Zhao, D., Guasco, T. L., Ebben, C. J., Geiger, F. M., Bertram, T. H., Prather, K. A., and Grassian, V. H.: Size-Dependent Changes in Sea Spray Aerosol Composition and Properties with Different Seawater Conditions, Environ. Sci. Technol., 47, 5603–5612, https://doi.org/10.1021/es400416g, 2013.

Benner, R. E., Barber, P. W., Owen, J. F., and Chang, R. K.: Observation of Structure Resonances in the Fluorescence Spectra from Microspheres, Phys. Rev. Lett., 44, 475–478, https://doi.org/10.1103/PhysRevLett.44.475, 1980.

Burgos, M. A., Andrews, E., Titos, G., Benedetti, A., Bian, H., Buchard, V., Curci, G., Kipling, Z., Kirkevåg, A., Kokkola, H., Laakso, A., Letertre-Danczak, J., Lund, M. T., Matsui, H., Myhre, G., Randles, C., Schulz, M., Van Noije, T., Zhang, K., Alados-Arboledas, L., Baltensperger, U., Jefferson, A., Sherman, J., Sun, J., Weingartner, E., and Zieger, P.: A global model–measurement evaluation of particle light scattering coefficients at elevated relative humidity, Atmos. Chem. Phys., 20, 10231–10258, https://doi.org/10.5194/acp-20-10231-2020, 2020.

Cai, C. and Zhao, C.: Optical levitation measurement on hygroscopic behaviour and SVOC vapour pressure of single organic/inorganic aqueous aerosol, Atmos. Environ., 189, 50–60, https://doi.org/10.1016/j.atmosenv.2018.06.040, 2018.

Cai, C., Miles, R. E. H., Cotterell, M. I., Marsh, A., Rovelli, G., Rickards, A. M. J., Zhang, Y., and Reid, J. P.: Comparison of Methods for Predicting the Compositional Dependence of the Density and Refractive Index of Organic–Aqueous Aerosols, J. Phys. Chem. A, 120, 6604–6617, https://doi.org/10.1021/acs.jpca.6b05986, 2016.

Clegg, S. L. and Wexler, A. S.: Densities and Apparent Molar Volumes of Atmospherically Important Electrolyte Solutions. 1. The Solutes H_2SO_4, HNO_3, HCl, Na_2SO_4, $NaNO_3$, NaCl, $(NH_4)_2SO_4$, NH_4NO_3, and NH_4Cl from 0 to 50 °C, Including Extrapolations to Very Low Temperature and to the Pure Liquid State, and $NaHSO_4$, NaOH, and NH_3 at 25 °C, J. Phys. Chem. A, 115, 3393–3460, https://doi.org/10.1021/jp108992a, 2011.

Cotterell, M. I., Willoughby, R. E., Bzdek, B. R., Orr-Ewing, A. J., and Reid, J. P.: A complete parameterisation of the relative humidity and wavelength dependence of the refractive index of hygroscopic inorganic aerosol particles, Atmos. Chem. Phys., 17, 9837–9851, https://doi.org/10.5194/acp-17-9837-2017, 2017.

de Leeuw, G., Andreas, E. L., Anguelova, M. D., Fairall, C. W., Lewis, E. R., O'Dowd, C., Schulz, M., and Schwartz, S. E.: Production flux of sea spray aerosol, Rev. Geophys., 49, RG2001, https://doi.org/10.1029/2010RG000349, 2011.

Gantt, B. and Meskhidze, N.: The physical and chemical characteristics of marine primary organic aerosol: a review, Atmos. Chem. Phys., 13, 3979–3996, https://doi.org/10.5194/acp-13-3979-2013, 2013.

Ghan, S. J. and Zaveri, R. A.: Parameterization of optical properties for hydrated internally mixed aerosol, J. Geophys. Res., 112, D10201, https://doi.org/10.1029/2006JD007927, 2007.

Haywood, J. M., Ramaswamy, V., and Soden, B. J.: Tropospheric Aerosol Climate Forcing in Clear-Sky Satellite Observations over the Oceans, Science, 283, 1299–1303, https://doi.org/10.1126/science.283.5406.1299, 1999.

He, X., Bai, Y., Pan, D., Tang, J., and Wang, D.: Atmospheric correction of satellite ocean color imagery using the ultraviolet wavelength for highly turbid waters, Opt. Express, 20, 20754-20770, https://doi.org/10.1364/OE.20.020754, 2012.

Janz, G. J.: Molten Salts Handbook, Academic Press, 588 pp, ISBN 978-0-12-395642-2, 1967.Kahn, R. A., Gaitley, B. J., Garay, M. J., Diner, D. J., Eck, T. F., Smirnov, A., and Holben, B. N.: Multiangle Imaging SpectroRadiometer global aerosol product assessment by comparison with the Aerosol Robotic Network, J. Geophys. Res., 115, D23209, https://doi.org/10.1029/2010JD014601, 2010.

Keene, W. C., Maring, H., Maben, J. R., Kieber, D. J., Pszenny, A. A. P., Dahl, E. E., Izaguirre, M. A., Davis, A. J., Long, M. S., Zhou, X., Smoydzin, L., and Sander, R.: Chemical and physical characteristics of nascent aerosols produced by bursting bubbles at a model air-sea interface, J. Geophys. Res., 112, D21202, https://doi.org/10.1029/2007JD008464, 2007.

Kleefeld, C., O'Dowd, C. D., O'Reilly, S., Jennings, S. G., Aalto, P., Becker, E., Kunz, G., and de Leeuw, G.: Relative contribution of submicron and supermicron particles to aerosol light scattering in the marine boundary layer, J. Geophys. Res., 107, 8103, https://doi.org/10.1029/2000JD000262, 2002.

Lewis, E. R. and Schwartz, S. E.: Sea Salt Aerosol Production: Mechanisms, Methods, Measurements and Models, American Geophysical Union, 432 pp., ISBN 978-0-875-90417-7, 2004.

Ming, Y. and Russell, L. M.: Predicted hygroscopic growth of sea salt aerosol, J. Geophys. Res., 106, 28259–28274, https://doi.org/10.1029/2001JD000454, 2001.

Moise, T., Flores, J. M., and Rudich, Y.: Optical Properties of Secondary Organic Aerosols and Their Changes by Chemical Processes, Chem. Rev., 115, 4400–4439, https://doi.org/10.1021/cr5005259, 2015.

Murphy, D. M., Anderson, J. R., Quinn, P. K., McInnes, L. M., Brechtel, F. J., Kreidenweis, S. M., Middlebrook, A. M., Pósfai, M., Thomson, D. S., and Buseck, P. R.: Influence of sea-salt on aerosol radiative properties in the Southern Ocean marine boundary layer, Nature, 392, 62–65, https://doi.org/10.1038/32138, 1998.

Myhre, G., Samset, B. H., Schulz, M., Balkanski, Y., Bauer, S., Berntsen, T. K., Bian, H., Bellouin, N., Chin, M., Diehl, T., Easter, R. C., Feichter, J., Ghan, S. J., Hauglustaine, D., Iversen, T., Kinne, S., Kirkevåg, A., Lamarque, J.-F., Lin, G., Liu, X., Lund, M. T., Luo, G., Ma, X., Van Noije, T., Penner, J. E., Rasch, P. J., Ruiz, A., Seland, Ø., Skeie, R. B., Stier, P., Takemura, T., Tsigaridis, K., Wang, P., Wang, Z., Xu, L., Yu, H., Yu, F., Yoon, J.-H., Zhang, K., Zhang, H., and Zhou, C.: Radiative forcing of the direct aerosol effect from AeroCom Phase II simulations, Atmos. Chem. Phys., 13, 1853–1877, https://doi.org/10.5194/acp-13-1853-2013, 2013.

O'Dowd, C. D. and de Leeuw, G.: Marine aerosol production: a review of the current knowledge, Philos. T. R. Soc. A., 365, 1753–1774, https://doi.org/10.1098/rsta.2007.2043, 2007.

O'Dowd, C. D., Facchini, M. C., Cavalli, F., Ceburnis, D., Mircea, M., Decesari, S., Fuzzi, S., Yoon, Y. J., and Putaud, J.-P.: Biogenically driven organic contribution to marine aerosol, Nature, 431, 676–680, https://doi.org/10.1038/nature02959, 2004.

Preston, T. C. and Reid, J. P.: Accurate and efficient determination of the radius, refractive index, and dispersion of weakly absorbing spherical particle using whispering gallery modes, J. Opt. Soc. Am. B, 30, 2113-2122, https://doi.org/10.1364/JOSAB.30.002113, 2013.

Qiu, J., He, B., Zhang, L., Cheng, M., Guo, S., Fan, C., and Zhao, C.: Hygroscopic behavior of sea spray aerosols in offshore waters and open sea areas investigated with aerosol optical tweezers, Atmos. Environ., 321, 120360, https://doi.org/10.1016/j.atmosenv.2024.120360, 2024.

Quinn, P. K., Coffman, D. J., Johnson, J. E., Upchurch, L. M., and Bates, T. S.: Small fraction of marine cloud condensation nuclei made up of sea spray aerosol, Nat. Geosci., 10, 674–679, https://doi.org/10.1038/ngeo3003, 2017.

Reich, O., Gleichweit, M. J., David, G., Leemann, N., and Signorell, R.: Hygroscopic growth of single atmospheric sea salt aerosol particles from mass measurement in an optical trap, Environ. Sci.: Atmos., 3, 695–707, https://doi.org/10.1039/D2EA00129B, 2023.

Rhein, M., S.R. Rintoul, S. Aoki, E. Campos, D. Chambers, R.A. Feely, S. Gulev, G.C. Johnson, S.A. Josey, A. Kostianoy, C. Mauritzen, D. Roemmich, L.D. Talley and F. Wang: Observations: Ocean. In: Climate Change 2013: The Physical Science Basis. Contribution of Working Group I to the Fifth Assessment Report of the Intergovernmental Panel on Climate Change [Stocker, T.F., D. Qin, G.-K. Plattner, M. Tignor, S.K. Allen, J. Boschung, A. Nauels, Y. Xia, V. Bex

and P.M. Midgley (eds.)]. Cambridge University Press, Cambridge, United Kingdom and New York, NY, USA, 255-316, 2013.

Richter, D. H. and Veron, F.: Ocean spray: An outsized influence on weather and climate, Phys. Today, 69, 34–39, https://doi.org/10.1063/PT.3.3363, 2016.

Sayer, A. M., Smirnov, A., Hsu, N. C., and Holben, B. N.: A pure marine aerosol model, for use in remote sensing applications, J. Geophys. Res., 117, D05213, https://doi.org/10.1029/2011JD016689, 2012.

Shepherd, R. H., King, M. D., Marks, A. A., Brough, N., and Ward, A. D.: Determination of the refractive index of insoluble organic extracts from atmospheric aerosol over the visible wavelength range using optical tweezers, Atmos. Chem. Phys., 18, 5235–5252, https://doi.org/10.5194/acp-18-5235-2018, 2018.

Shettle, E. P. and Fenn, R. W.: Models for the Aerosols of the Lower Atmosphere and the Effects of Humidity Variations on Their Optical Properties, Environ. Res. Pap. 676, Air Force Geophys. Lab., AFGL-TR-79-0214, 1979.

Tang, I. N. and Munkelwitz, H. R.: Water activities, densities, and refractive indices of aqueous sulfates and sodium nitrate droplets of atmospheric importance, J. Geophys. Res., 99, 18801–18808, https://doi.org/10.1029/94JD01345, 1994.

Tang, I. N., Tridico, A. C., and Fung, K. H.: Thermodynamic and optical properties of sea salt aerosols, J. Geophys. Res., 102, 23269–23275, https://doi.org/10.1029/97JD01806, 1997.

Toon, O. B., Pollack, J. B., and Khare, B. N.: The optical constants of several atmospheric aerosol species: Ammonium sulfate, aluminum oxide, and sodium chloride, J. Geophys. Res., 81, 5733–5748, https://doi.org/10.1029/JC081i033p05733, 1976.

Volz, F. E.: Infrared Refractive Index of Atmospheric Aerosol Substances, Appl. Opt., 11, 755-759, https://doi.org/10.1364/AO.11.000755, 1972.

Wang, W. and Rood, M. J.: Real refractive index: Dependence on relative humidity and solute composition with relevancy to atmospheric aerosol particles, J. Geophys. Res., 113, D23305, https://doi.org/10.1029/2008JD010165, 2008.

Wang, Z., Bi, L., Yi, B., and Zhang, X.: How the Inhomogeneity of Wet Sea Salt Aerosols Affects Direct Radiative Forcing, Geophys. Res. Lett., 46, 1805–1813, 2019.

Wexler, A. S. and Clegg, S. L.: Atmospheric aerosol models for systems including the ions H^+, NH_4^+, Na^+, SO_4^{2-}, NO_3^-, Cl^-, Br^-, and H_2O, J. Geophys. Res., 107, ACH 14-1-ACH 14-14, https://doi.org/10.1029/2001JD000451, 2002.

Zarzana, K. J., Cappa, C. D., and Tolbert, M. A.: Sensitivity of Aerosol Refractive Index Retrievals Using Optical Spectroscopy, Aerosol Sci. Tech., 48, 1133–1144, https://doi.org/10.1080/02786826.2014.963498, 2014.

Zhao, G., Zhao, C., Kuang, Y., Tao, J., Tan, W., Bian, Y., Li, J., and Li, C.: Impact of aerosol hygroscopic growth on retrieving aerosol extinction coefficient profiles from elastic-backscatter lidar signals, Atmos. Chem. Phys., 17, 12133–12143, https://doi.org/10.5194/acp-17-12133-2017, 2017.

Zhao, G., Tan, T., Zhao, W., Guo, S., Tian, P., and Zhao, C.: A new parameterization scheme for the real part of the ambient urban aerosol refractive index, Atmos. Chem. Phys., 19, 12875–12885, https://doi.org/10.5194/acp-19-12875-2019, 2019.